PNAS RESEARCH ARTICLE | APPLIED PHYSICAL SCIENCES
POPULATION BIOLOGY

OPEN ACCESS

Heterogeneous changes in mobility in response to the SARS-CoV-2 Omicron BA.2 outbreak in Shanghai

Juanjuan Zhang[a,1], Suoyi Tan[b,1], Cheng Peng[a], Xiangyanyu Xu[a], Mengning Wang[b], Wanying Lu[a], Yanpeng Wu[a], Bin Sai[b], Mengsi Cai[b], Allisandra G. Kummer[c], Zhiyuan Chen[a], Junyi Zou[a], Wenxin Li[a], Wen Zheng[a], Yuxia Liang[a], Yuchen Zhao[a], Alessandro Vespignani[d], Marco Ajelli[c,2], Xin Lu[b,2,3], and Hongjie Yu[a,2,3]

Edited by Andrea Rinaldo, Ecole Polytechnique Federale de Lausanne, Lausanne, Switzerland; received April 24, 2023; accepted September 12, 2023

The coronavirus disease 2019 (COVID-19) pandemic and the measures taken by authorities to control its spread have altered human behavior and mobility patterns in an unprecedented way. However, it remains unclear whether the population response to a COVID-19 outbreak varies within a city or among demographic groups. Here, we utilized passively recorded cellular signaling data at a spatial resolution of 1 km × 1 km for over 5 million users and epidemiological surveillance data collected during the severe acute respiratory syndrome coronavirus 2 (SARS-CoV-2) Omicron BA.2 outbreak from February to June 2022 in Shanghai, China, to investigate the heterogeneous response of different segments of the population at the within-city level and examine its relationship with the actual risk of infection. Changes in behavior were spatially heterogenous within the city and population groups and associated with both the infection incidence and adopted interventions. We also found that males and individuals aged 30 to 59 y old traveled more frequently, traveled longer distances, and their communities were more connected; the same groups were also associated with the highest SARS-CoV-2 incidence. Our results highlight the heterogeneous behavioral change of the Shanghai population to the SARS-CoV-2 Omicron BA.2 outbreak and the effect of heterogenous behavior on the spread of COVID-19, both spatially and demographically. These findings could be instrumental for the design of targeted interventions for the control and mitigation of future outbreaks of COVID-19, and, more broadly, of respiratory pathogens.

human mobility | COVID-19 | mobile phones

Significance

Our study utilized passively recorded cellular signaling data and epidemiological surveillance data to investigate the changes of human mobility to a COVID-19 outbreak at an unprecedented within-city level and examine its relationship with the actual risk of infection. Our findings highlight the heterogeneous behavioral change of the Shanghai population to the 2022 severe acute respiratory syndrome coronavirus 2 (SARS-CoV-2) Omicron BA.2 outbreak and the effect of heterogenous behavior on the SARS-CoV-2 spread, both spatially and demographically. The implications of our findings could be instrumental to inform spatially targeted interventions at the within-city scale to mitigate possible new surges of COVID-19 cases as well as fostering preparedness for future respiratory infectious disease outbreaks.

Following the initial COVID-19 wave in early 2020, mainland China adopted stringent measures, often referred to as the "zero-COVID" strategy, to curb COVID-19 outbreaks (1). This approach effectively minimized severe acute respiratory syndrome coronavirus 2 (SARS-CoV-2) transmission in China until the emergence of the Omicron variant in late 2021 (2). Subsequently, several Omicron outbreaks occurred, with a significant outbreak in Shanghai, identified in March 2022, accounting for over 600,000 confirmed infections (3). Comprehensive PCR testing, citywide lockdowns, and additional measures to restrict interpersonal interactions were implemented, ultimately containing the outbreak by June 2022. China eventually abandoned the zero-COVID policy 6 mo later (4).

Human mobility patterns, ranging from international travel to daily commuting, significantly influence the spread of infectious diseases due to the nature of interpersonal interactions (5–10). Recent years have seen an exponential growth in geolocated datasets that provide unprecedented levels of detail to quantify human mobility (10–19). In particular, data collected from mobile devices have extensively been used in the early phase of the COVID-19 pandemic to investigate transmission dynamics, estimate changes in contact and mobility patterns as a result of public health interventions, and forecast epidemic spread (11, 13, 18–21). However, limitations in the epidemiological and mobility data analyzed (e.g., varying COVID-19 reporting rates by age, incomplete demographic information for individual travel trajectories) have left several key questions regarding the relationships between epidemic spread, implemented interventions, and human behavior and mobility unanswered. In particular, it remains unclear whether population responses to a COVID-19 outbreak, as measured by travel frequency, distance traveled, and population connectivity, vary within a city (e.g., by district area) or among demographic groups (e.g., by age and sex) (22).

To address these knowledge gaps, we utilized passively recorded Cellular Signaling Data (CSD) from over 5 million users (approximately 20% of Shanghai's population) and epidemiological surveillance data collected during the SARS-CoV-2 Omicron BA.2 outbreak in Shanghai. The exceptional scale and resolution of the human mobility data enabled us to analyze micro-level changes in mobility within the city and among different

Competing interest statement: H.Y. has received research funding from Sanofi Pasteur, GlaxoSmithKline, Yichang HEC Changjiang, Shanghai Roche Pharmaceutical Company, and SINOVAC Biotech Ltd. M.A. has received research funding from Seqirus. None of those research funding is related to this work. All other authors declare no competing interests.

This article is a PNAS Direct Submission.

[1]J. Zhang and S.T. contributed equally to this work.

[2]M.A., X.L., and H.Y. contributed equally to this work.

[3]To whom correspondence may be addressed. Email: xin.lu.lab@outlook.com or yhj@fudan.edu.cn.

This article contains supporting information online at https://www.pnas.org/lookup/suppl/doi:10.1073/pnas.2306710120/-/DCSupplemental.

Published October 12, 2023.

population groups (e.g., age and sex). Additionally, the repeated city-wide PCR screenings provided an opportunity to examine the association between these behavioral shifts and high-quality epidemiological data in the unique context of Shanghai's 2022 Omicron BA.2 outbreak.

Results

Omicron BA.2 Outbreak in Shanghai and Public Health Response. In early March 2022, Shanghai experienced a significant outbreak of the SARS-CoV-2 Omicron BA.2 variant, which rapidly spread among its 25 million residents. Throughout the outbreak, authorities conducted multiple mass PCR screenings; by the end of the outbreak on June 30, 2022, they had identified a total of 627,132 SARS-CoV-2 infections (Fig. 1*A*). During the outbreak's initial phase, authorities implemented grid management and partial lockdowns at the subdistrict level. On March 28, eastern Shanghai, consisting of subdistricts east of the Huangpu River (*SI Appendix*, Fig. S1*A*), entered a population-wide lockdown, followed by a citywide lockdown for the rest of Shanghai on April 1. The citywide lockdown was lifted entirely on June 1, 2022, when the daily number of newly reported infections dropped to 10. Further information on the public health response can be found in *Materials and Methods*, *SI Appendix*, Fig. S2 and Table S2.

Changes in Frequency of Travel, Distance Traveled, and Mobility Network Community Structure over the Course of the Outbreak. We quantified spontaneous and intervention-induced behavioral changes of the Shanghai population in terms of their daily mobility patterns based on CSD. Subsequently, we employed the Infomap method (23) to identify community structures within the mobility networks. Further details can be found in the *Materials and Methods* section and *SI Appendix*, section 1.

Pre-Outbreak Phase. During the 2 wk before the Omicron outbreak began, we estimated an average of 1.365 trips per person per day, corresponding to a total of 7.03 million trips per day (Fig. 1*A*). Approximately, 33.4% of the cells in the central urban areas accounted for 80% of the total mobility in Shanghai (Fig. 1*B*). The median distance traveled was 6.035 km; trips within 10 km accounted for 66.7% of all trips (Fig. 1 *C* and *D*). We identified 40 total communities, with a sizable core community (~8% of Shanghai's land area) at the city's center, surrounded by peripheral communities outside the Shanghai metropolitan area (Fig. 2*A* and *SI Appendix*, Fig. S3 *A* and *F*).

Targeted Interventions Phase. After the implementation of public places closures, school closures, mass screenings, and travel restrictions beginning on March 2, the number of daily trips per person decreased from 1.365 to 0.895 (Fig. 1*A*). Long-distance trips, defined as those exceeding 30 km, experienced the most substantial decrease, dropping by approximately 47.5% compared to the pre-outbreak phase. This reduction brought the median travel distance down to 5.090 km ($P < 0.0001$; see Fig. 1 *C* and *D* and *SI Appendix*, Fig. S5*A*). By the end of the targeted interventions phase, the number of communities within the mobility network had increased to around 50 (Fig. 2*B* and *SI Appendix*, Fig. S3 *B* and *F*).

Citywide Lockdown Phase. After a citywide lockdown was implemented on April 1, mobility decreased by 87.3% compared to the pre-outbreak phase and remained stable for about a month (Fig. 1*A*). The median travel distance decreased to 1.205 km ($P < 0.0001$), with 79.0% of trips spanning less than 3 km (Fig. 1 *C* and *D* and *SI Appendix*, Fig. S5*A*). The initial 40 communities fragmented into 221 smaller ones, effectively dismantling the core-periphery structure that connected various parts of the city (Fig. 2*C* and *SI Appendix*, Fig. S3 *C* and *F*).

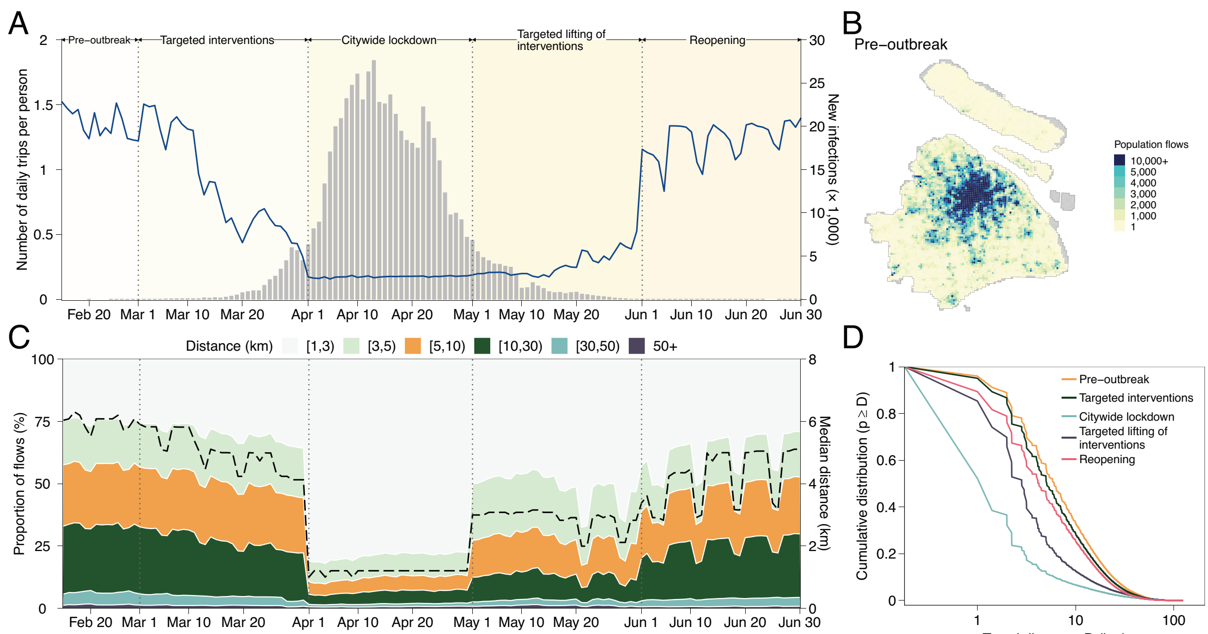

Fig. 1. Changes in population flows and travel distance in Shanghai. (*A*) Changes in number of daily trips per person and number of new infections reported from February 15 to June 30, 2022. Grey bars represent the daily reported infections. (*B*) The geographic distribution of population trips during the pre-outbreak phase. The color intensity represents the number of daily trips occurred in each cell, which is calculated as the sum of the incoming trips of a given cell and the outgoing trips of that same cell. (*C*) The proportion of daily trips by different distances travelled (filled colors) and median distance of daily trips (dotted line) from February 15 to June 30, 2022. (*D*) The cumulative probability distribution against distance (log) of daily trips across all five phases, where *P* is defined as the probability of traveling between locations exceeding a certain distance. Each line represents the probability distribution per phase.

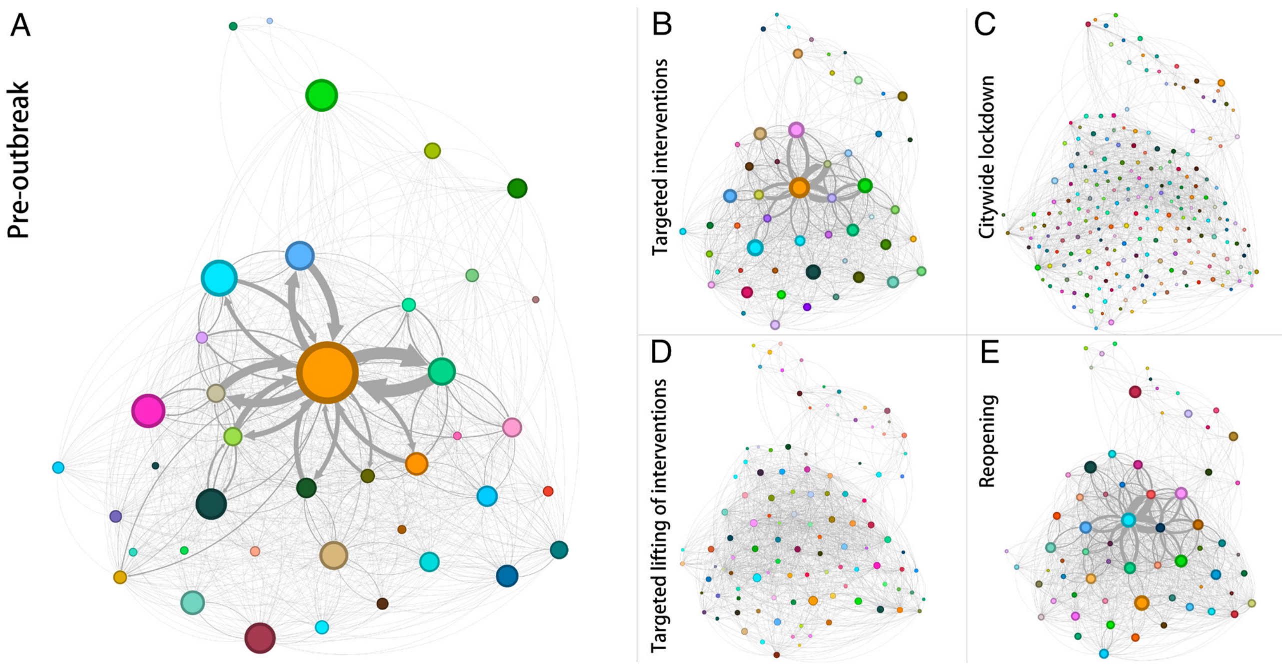

Fig. 2. The network structural changes during each phase. (*A*–*E*) Community structures during the pre-outbreak, targeted interventions, citywide lockdown, targeted lifting of interventions, and reopening phases, respectively. Each node corresponds to a community, and the center of the node coincides with the centroid of the community. The size of each node is proportional to the area (number of cells) of the community. The width of the directed arrow is proportional to the flows between communities. More information about flows within the same community can be found in *SI Appendix*, Fig. S4.

Targeted Lifting of Interventions Phase. Coinciding with the partial lifting of interventions on May 1, data revealed a gradual increase in mobility, reaching 19.3% of pre-outbreak levels (Fig. 1*A*). Meanwhile, the median distance traveled per day rose to approximately half of what it was in the pre-outbreak phase ($P < 0.0001$; see Fig. 1 *C* and *D*). The number of distinct communities decreased to 109 with a ramping up of the strength of connections across different cells of the city (Fig. 2*D* and *SI Appendix*, Fig. S3 *D* and *F*).

Reopening Phase. Upon lifting most interventions on June 1, we observed an immediate resurgence in mobility flows, reaching 90.5% of pre-outbreak levels in under a week (Fig. 1*A*). Short-distance trips (<3 km) increased more rapidly, exceeding pre-outbreak levels, while long-distance trips only recovered to about half of their pre-outbreak frequency. By June 30, the median trip distance had just returned to its level during targeted interventions (5.105 km vs. 5.090 km), although the number of daily trips had almost reverted to pre-outbreak figures (Fig. 1*A* and *SI Appendix*, Fig. S5*A*). Ongoing mandatory COVID-19 tests for travel outside residential areas within the city, along with additional policies, prevented the community structure from fully reverting to its pre-outbreak state (54 vs. 40 communities) (Fig. 2*E* and *SI Appendix*, Fig. S3 *E* and *F*).

Spatially Heterogeneous Impact of the Epidemic and the Adopted Interventions on Population Mobility. Before the lockdown of eastern Shanghai, mobility reductions were heterogeneous across cells, with larger reductions observed in cells severely hit by the epidemic (Pearson $\rho = 0.115$, $P < 0.001$; see Fig. 3 *A* and *B*). Cells with more than 50 infections exhibited an average mobility reduction of 78.7%, while the reduction was just 13.0% for cells without infections ($P < 0.0001$; see Fig. 3*B*). During the targeted lifting of interventions phase, particularly after May 16 when public transportation began to resume, strict mobility-restricting policies persisted in high-risk areas with sustained incidence rates. In contrast, substantial rebounds in mobility were observed in low-risk cells, encompassing both suburban and rural areas of Shanghai (Fig. 3 *C* and *D*). The recovery of mobility was significantly associated with the number of new infections reported in the cells (Pearson $\rho = -0.096$, $P < 0.001$). Specifically, cells with more than 50 infections had a very low recovery of mobility (12.6% on average), while the recovery reached 84.1% for cells without infections ($P < 0.0001$; see Fig. 3*D*). These analyses were performed under the assumption that the mobility of the population in a given day was affected by the status of the epidemic and interventions in the same day.

Changes in Frequency of Travel, Distance Traveled, and Mobility Network Community Structure by Demographic Characteristics. To calculate the mobility and community structure by demographic characteristics, we analyzed mobility flows separately by age group and sex. The range of mobility was measured by the proportion of the area covered by the top 10 communities (α), the total number of identified communities (NC), and the number of communities covering more than 10 cells $\left(NC_{g\geq 10}\right)$. Based on the individual-level data of infected individuals reported between March 1 and March 25 (targeted interventions phase), we analyzed the relationship between mobility patterns and the incidence of SARS-CoV-2 as well as the number of cells with reported infections by demographic characteristics.

During the pre-outbreak phase, the number of daily trips per person and distance travelled were highest for adults aged 30 to 59 y (1.457 trips, $P < 0.0001$; 6.195 km, $P < 0.0001$) and lowest for older adults aged 70+ (0.596 trips, $P < 0.0001$; 4.350 km, $P < 0.0001$) (Fig. 4*A* and *SI Appendix*, Fig. S5*B* and Tables S4 and S5). During the targeted interventions phase, for all age groups, higher mobility was significantly correlated with higher infection incidence (Pearson $\rho = 0.904$, $P = 0.035$), and longer travel distances were correlated with larger infected areas (Pearson $\rho = 0.894$, $P = 0.040$; *SI Appendix*, Tables S7 and S8). Specifically, compared

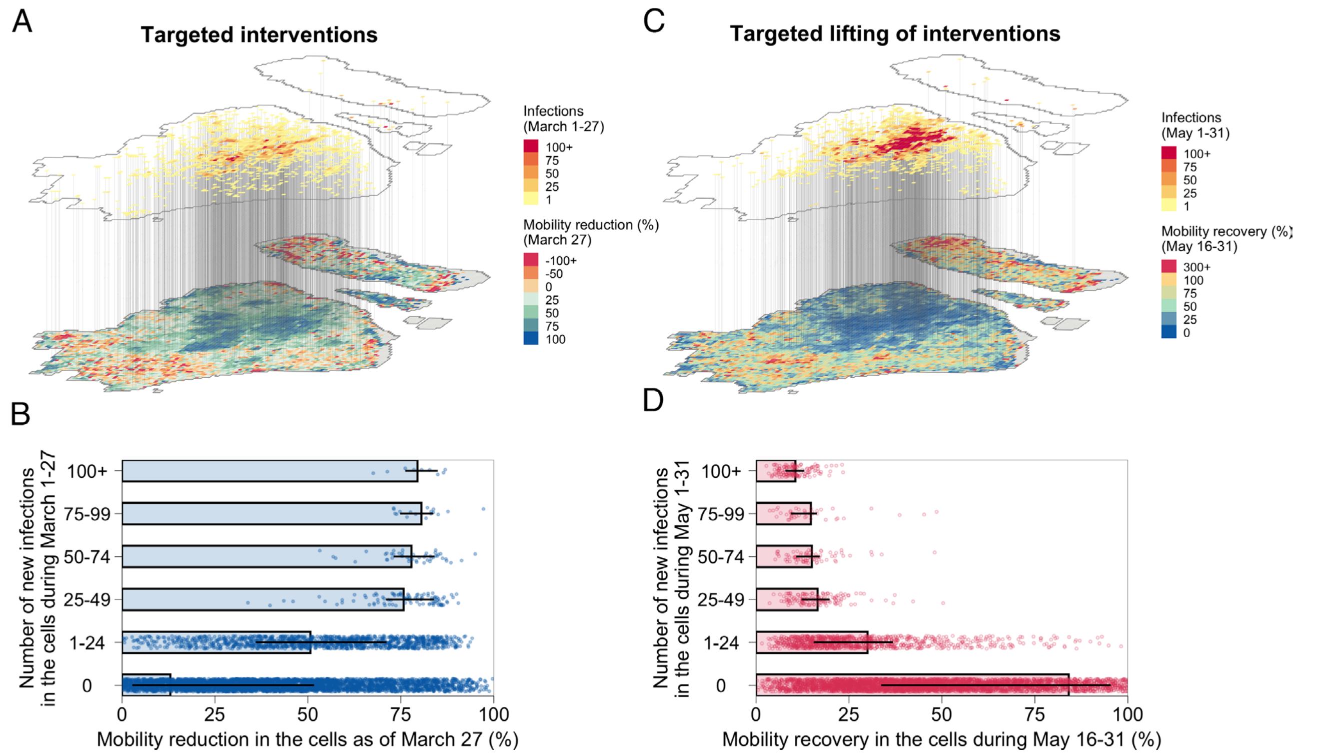

Fig. 3. Impact of epidemic and interventions on the changes in mobility. (*A*) The geographic distribution of infections and mobility reduction during the targeted interventions phase. The upper map represents the cumulative number of infections at the grid level as of March 27 (i.e., before the lockdown of eastern Shanghai). The lower map represents the mobility reduction, which is computed as the subtraction of daily trips on March 27 from the pre-outbreak mobility level, divided by the pre-outbreak mobility level. (*B*) The mobility reduction as a function of the number of new infections in the cells during the targeted interventions phase. The bar represents the mean value, while the horizontal line represents 50% quantile intervals. Each dot corresponds to the result for each cell. Note that the dots with a negative mobility reduction were not displayed. (*C*) The geographic distribution of infections and mobility recovery during the targeted lifting of interventions phase. The upper map represents the cumulative number of infections at the grid level from May 1 to May 31. The lower map represents the mobility recovery, which is computed as the daily average trips between May 16 and May 31 divided by the pre-outbreak mobility level. The recovery may be beyond 100% if the daily trips during May 16 and May 31 are higher than the pre-outbreak mobility level. (*D*) The same as panel *B*, but for the targeted lifting of interventions phase. Note that the dots with a mobility recovery beyond 100% were not displayed.

with middle-aged adults aged 30 to 59, individuals 70+ y old travelled 62.8% less frequently (P < 0.0001) and 25.9% shorter distances (P < 0.0001), and correspondingly had a 44.3% lower incidence (P < 0.0001) and 71.6% less infected cells (P < 0.0001). Older adults aged 70+ also showed most reduction of mobility in this phase (P < 0.0001; *SI Appendix*, Fig. S5*C*). Neither travel distance nor travel volume was obviously different across all age groups during the citywide lockdown, although the difference is statistically significant among all age groups due to large sample size; however, they quickly rebounded to the pre-outbreak level during the reopening phase, of which individuals 70+ y old had the lowest mobility recovery (P < 0.0001; see Fig. 4 *B* and *C* and *SI Appendix*, Fig. S5*C*). Different age groups also presented various mobility network patterns across phases (Fig. 4 *D*–*G*). Middle-aged groups (30 to 59 y old) visited substantially more locations than younger or older groups (P < 0.0001); for example, the average degree $\langle k \rangle$ for middle-aged groups was 40 times that for 16 to 18 y old. Similarly, the mobility networks of middle-aged groups were more densely connected, with higher transitivity (adjacent neighboring locations, P < 0.0001) (*SI Appendix*, Table S6). This difference was more prominent in community structures. For example, younger and older groups had smaller and less connected communities ($\alpha = 5.913\%$, NC = 319; $\alpha = 6.527\%$, NC = 369, respectively), whereas middle-aged groups had fewer well-connected communities covering large areas ($\alpha = 37.250\%$, P < 0.0001; NC = 141, P < 0.0001) (*SI Appendix*, Fig. S6). The connections of the mobility networks for all age groups were reduced by lockdown and were not fully recovered during the reopening phase (Fig. 4 *E* and *F*).

Males were associated with longer travel distance (6.080 km vs. 5.815 km, P < 0.0001) and higher daily trips (1.446 trips vs. 1.212 trips, P < 0.0001) than females during the pre-outbreak phase (Fig. 4*A* and *SI Appendix*, Fig. S5*D* and Tables S4 and S5). Males travelled 30.3% more frequently (P < 0.0001) and 3.9% longer distances (P < 0.0001), which corresponded to 9.7% higher incidence (P < 0.0001) and 7.3% more infected cells (P = 0.089) than females during the targeted interventions phase (*SI Appendix*, Tables S7 and S8). Males also showed less reduction of mobility in this phase (P < 0.0001; *SI Appendix*, Fig. S5*E*). The mobility patterns remained comparable across sexes during citywide lockdown (Fig. 4*B*). Females had a lower recovery of mobility during the reopening phase (P < 0.0001; *SI Appendix*, Fig. S5*E*). Sex was also a strong factor affecting the mobility network patterns. During the pre-outbreak phase, males had a greater range of mobility and smaller community sizes ($\alpha = 37.161\%$, NC = 147) than females ($\alpha = 31.033\%$, NC = 207), indicating that males traveled more frequently (P < 0.0001) and distantly (P < 0.0001) than females. This difference persisted across all epidemic phases (Fig. 4 *D*–*F* and *SI Appendix*, Fig. S6).

Additional Analyses at Different Spatial and Temporal Resolutions. Additionally, we compared changes in frequency of daily trips at the grid, subdistrict, and district levels. Trips between subdistricts or districts exhibited higher reduction in mobility during the citywide lockdown for the subdistrict (91.3%, P < 0.0001) and district levels (95.4%, P < 0.0001) compared to

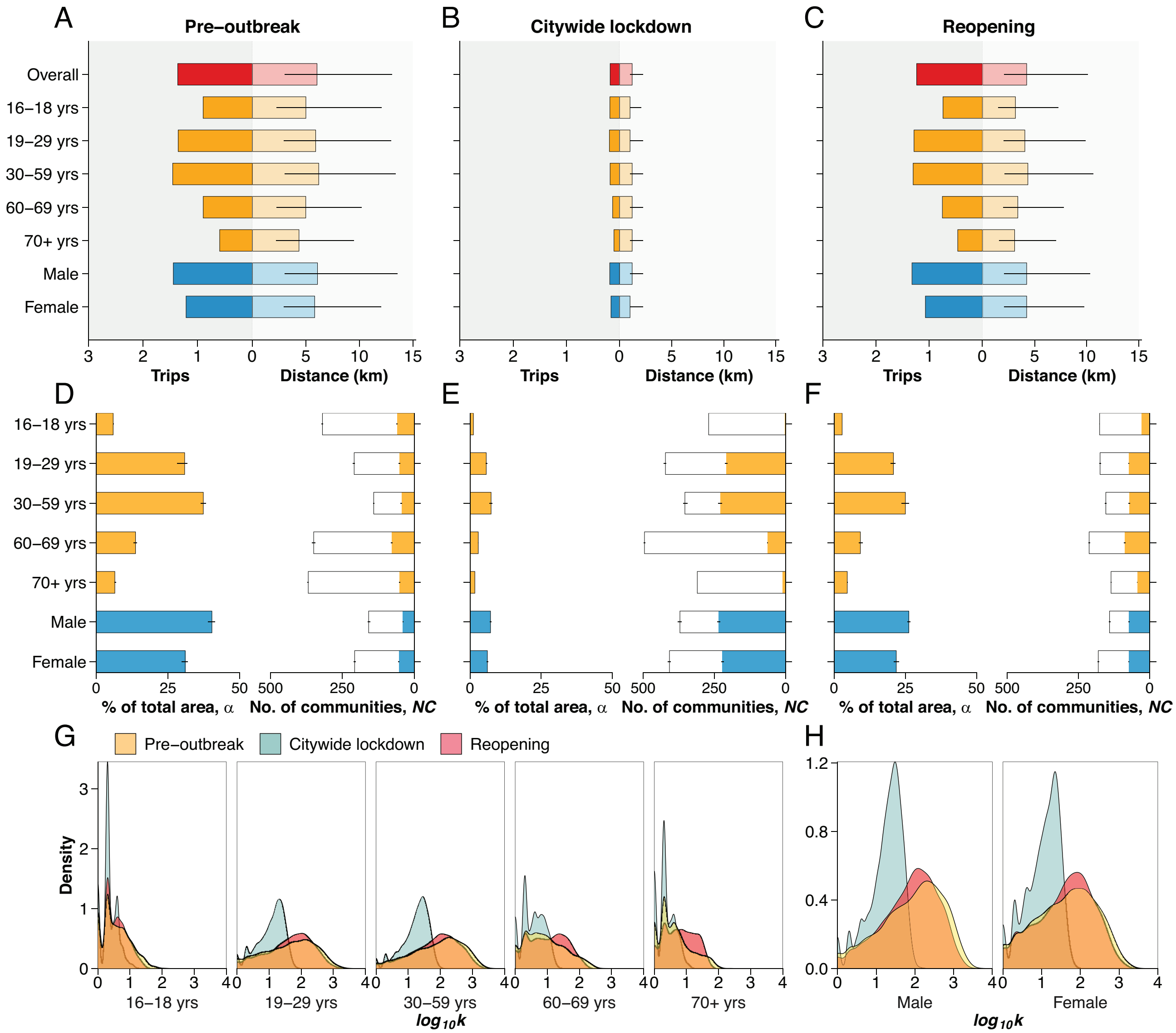

Fig. 4. Changes in frequency, distance, and community structures of mobility network by age and sex. (*A*–*C*) Mean number of daily trips per person and median distance travelled by age group and sex during the pre-outbreak, citywide lockdown, and reopening phases. The mean number of daily trips per person and 95% CIs on the mean are calculated by bootstrap sampling. The bar corresponds to the mean or median value, while the horizontal line represents 95% CI (quantile interval) for number of daily trips and 50% CI (quantile interval) for travel distance. The horizontal line for trips may not be visible due to very narrow CIs. Summary of frequency and distance across phases is shown in *SI Appendix*, Tables S4 and S5. (*D*–*F*) The left part of each panel represents the proportion α, i.e., the top-10 communities in terms of area (km^2) for each category to the total area (7,355 km^2). The right part of each panel represents the total number of identified communities NC, where the filled portions represent the number of communities that spans more than 10 cells $NC_{g\geq10}$. The community detection process was performed 100 times to calculate the average α, NC, $NC_{g\geq10}$ and their 95% CIs (quantile intervals). The bar corresponds to the mean value, while the horizontal line represents 95% CI. (*G* and *H*) The degree distribution of the mobility network across phases by age group and sex. Summary of the topological features of the mobility networks by age group and sex is shown in *SI Appendix*, Table S6.

the grid (1 km × 1 km cells) level (87.5%) (*SI Appendix*, Fig. S7*A* and Table S9). We also observed a less marked reopening rebound of the mobility, reaching 79.1% and 69.2% of the pre-outbreak flows, respectively, for the subdistrict (P < 0.0001) and district (P < 0.0001) levels compared to 91.2% at the grid level. We then compared the proportion of daily population flows at different spatial resolutions, including inter-flow and intra-flow, where the inter-flow denotes the population flows between cells (or subdistricts, districts) and the intra-flow represents population flows within the same cell (or subdistrict, district). Our results show significantly different patterns across different resolutions for each phase (P < 0.0001; *SI Appendix*, Fig. S7 *B*–*D*). Low-resolution mobility data may thus mask the variability in the dynamics of mobility flows.

We further investigated alterations in mobility and commuting patterns at various temporal resolutions. Trips to or from outside Shanghai are not considered in this study. The periodic weekly commuting pattern swiftly rebounded during the reopening phase, even though the frequency of travel, distance traveled, and community structure had not fully recovered. Notably, we observed significant differences in travel frequency, distance traveled, and community structure of mobility networks between weekdays and weekends as well as at different times of the day. For more details, refer to *SI Appendix*, section 4 and Figs. S7–S9 for details.

Discussion

Our analysis provided an in-depth assessment of the behavioral changes within the Shanghai population in response to the 2022 SARS-CoV-2 Omicron BA.2 outbreak, considering fine spatial and temporal scales as well as demographic characteristics.

Pre-outbreak mobility was unevenly distributed across the city, with 33.4% of cells located in the center of Shanghai accounting for 80% of all trips. This is consistent with the geographical distribution of population density in Shanghai. The crowd movement during the pre-outbreak phase reveals the specific socio-economic distribution and commuting patterns in Shanghai. Mobility reductions were also spatially heterogeneous from the targeting interventions phase through the reopening phase, as different policies were adopted according to the local epidemic situation. Larger reductions were measured in cells more severely hit by the epidemic. These findings hint to possible spontaneous behavioral changes where individuals witnessing a large number of infections reported in their cells might have limited their mobility beyond the mandated restrictions compared with those living in less affected cells. When the citywide lockdown entered into effect, the situation became homogenous as mobility reached its minimum level in all areas.

Throughout the outbreak, the frequency of travel and distance traveled generally adhered to the timeline of interventions implemented to combat the spread of SARS-CoV-2. Mobility reached its lowest level during the citywide lockdown phase, with an average of 0.174 trips per day per person and 1.205 km traveled. The community structure identified by the mobility flows followed the same pattern as well, with the population fragmenting into an increasing number of smaller communities as the level of intervention intensified. Mobility and community size quickly rebounded within the first week after interventions were lifted, although in the following month, they had not fully recovered to pre-outbreak levels. During the outbreak, changes in behavior were spatially heterogenous within the city and directly associated with both the epidemic situation and interventions. We observed that males and individuals aged 30 to 59 y old traveled more frequently, traveled longer distances, and their communities were more connected, which were associated with higher incidence of SARS-CoV-2 infections and larger infected areas.

In late May, public transportation was partially reopened, and individuals living in less affected cells were allowed conditional trips (e.g., one individual per household per day was allowed to buy necessities). During the reopening phase, we found that mobility quickly rebounded within the first week (although it did not return to the pre-outbreak level). This recovering trend is substantially different from some European and US locations where the rebound was much slower, possibly due to the persistence of the epidemic or different levels of lockdown fatigue (12, 17, 24, 25). Within the Shanghai population, we found a slower mobility recovery during reopening among older adults (70+ y), which suggests possible spontaneous choices to limit mobility to minimize the risk of infection given widespread information about the increased risk of developing severe symptoms by age if infected. At the same time, it is also possible that the policy of requiring negative PCR results within 72 h to travel within the city (but outside their residential area) may have contributed to a reduced mobility among older adults as they are less likely to use smart phones to show proof of negative test result (26).

One interesting aspect of our analysis is that we have observed a spatially heterogeneous response to the outbreak. Although this was already found in previous country-level analyses (17, 27–29), here we are observing marked differences at the within-city scale. Our analysis also shows that at the within-city scale, results are generally consistent if data are analyzed at 1-km^2 resolution or using administrative boundaries (e.g., district, subdistrict), although quantitative differences do exist, highlighting the importance of selecting the appropriate spatial level of aggregation of mobility data depending on the focus research question. Moreover, we found that interventions altered not only the number of trips but also their length. In particular, after the lockdown was lifted, we observed an increase in trips under 3 km as compared to pre-outbreak mobility. These heterogeneous patterns may be useful for informing spatially targeted interventions at the within-city scale. For example, targeted spatial distribution of vaccine doses and antiviral treatments, screening hubs, and lockdown areas that cover different spatial sizes could be instated depending on the mobility of the population.

While mobile phone data are widely used to quantify human mobility, there are potential sources of inaccuracy to consider, such as i) population representativeness (e.g., by age), ii) geographical coverage, and iii) heterogeneity in user activity. First, our study may be subject to selection bias, as we analyzed the mobility of mobile phone owners, which could exclude or underrepresent young children and older adults (*SI Appendix*, Fig. S1*H* and section 1). However, despite this affecting our population-level results, we have provided an assessment by age and sex that does not suffer from this bias. Second, we analyzed data representing approximately 20% of Shanghai's population, with a median coverage by subdistrict of 19.5% (interquartile range: 14.9 to 24.7%) (*SI Appendix*, Fig. S1*C*). Third, by relying on passively recorded CSD instead of actively recorded signals, we have mitigated the bias of heterogeneity in user activity. Another limitation is that the number of infections disaggregated by age and sex is available to us only until March 25, 2022. This constraint limited our comparison between epidemiological data and human mobility patterns with a stratification by sex and age to the initial phase of the outbreak. It is also possible that a mobile phone was used by more than one household member, thus affecting our results disaggregated by population characteristics. However, official statistics from the Ministry of Industry and Information Technology corroborate the immense ubiquity of mobile phones within Shanghai's population, with a staggering penetration rate of 178.1% as of 2022 (30). Furthermore, the prevalence of mobile payment systems in China has almost replaced the use of cash and necessitates users to link their authentic identity information with their cell phone numbers. Finally, it is important to remark that the analyzed mobility and epidemiological data are not linked at the individual level. As such, only population-level analyses were possible to connect the two datasets.

In summary, behavioral changes during the 2022 Omicron BA.2 outbreak were heterogeneous, both spatially and demographically. By shedding light on the varied responses among population groups, our findings can be instrumental in guiding the development of spatially targeted interventions to mitigate potential new surges in COVID-19 cases, as well as fostering preparedness for future respiratory infectious disease outbreaks.

Materials and Methods

Data Sources. ***Mobile phone data.*** CSD were provided by China Unicom, one of the largest national mobile carriers in China, which accounts for approximately one-third of all active mobile phone users in Shanghai. Active signaling data were recorded during events such as phone calls, text messages, device power on/off, or tower switches, while passive signaling data captured the user's location approximately every 30 min, provided the phone was turned on. The original CSD data include the timestamp of each event and a unique identifier for the mobile phone tower routing the activity. The demographic characteristics of each phone user are available to the service provider based on user registration information. The analyzed data have been anonymized and aggregated by the provider at a temporal resolution of 1 h, spatial resolution of 1 km × 1 km (grid level), and demographic characteristics (age and sex) of the phone users. Then, we received the data from the provider as a set of matrices containing the number of users traveling between each pair of cells for each population group (age, sex) and hour of the day. The data span from February 15, 2022, to June 30, 2022, and consist of an average of 5.04 million phone users (20% of the total population) per day throughout the study period.

Epidemiological data. Daily aggregated data on the number of infections and individual-level data (line list) of all SARS-CoV-2 infections were extracted from multiple publicly available official data sources (websites of municipal health commission and local government media) as detailed in our previous study (3). The resulting line list contains all reported infections with the following primary variables: date of official reporting, residential location (address, district, and subdistrict), age, and sex. The residential address of each reported infection is available throughout the study period (February 15, 2022, to June 30, 2022), while the age and sex information is available only for infected individuals reported between March 1 and March 25, 2022. To protect privacy, residential addresses of the infected individuals were first geocoded, then aggregated at the cell level, so that the number of infections can be linked with the population flows at the grid level.

Timeline of the Outbreak and Public Health Response. After the outbreak was initially reported on March 1, 2022, a series of non-pharmaceutical interventions (NPIs) were implemented to suppress transmission. Schools closed on March 12. From March 16 to 27, Shanghai introduced grid management at the subdistrict level by dividing subdistricts into high-risk and non-high-risk areas, based on factors such as the epidemiological situation (number of infections and cases), population density, social characteristics, and economic activity. High-risk areas underwent one or two rounds of population-wide PCR screening within 48 h, accompanied by lockdown orders. Non-high-risk areas conducted a single round of mass screening.

On March 28, eastern Shanghai (comprising subdistricts east of the Huangpu River; *SI Appendix*, Fig. S1*A*) entered a population-wide lockdown, followed by the rest of Shanghai on April 1 (citywide lockdown). Key enterprises and public transportation began resuming operations in May, with the citywide lockdown fully lifted on June 1. However, some restrictions persisted throughout June, limiting population movement. For instance, entering public places and transportation required proof of a negative PCR test result within 72 h, and restaurants prohibited dine-in service until June 29. Additional details on the public health response can be found in *SI Appendix*, Fig. S2 and Table S2.

Definition of the Five Phases of the Outbreak. For the purposes of this analysis, we categorized the outbreak into five phases based on the implemented interventions and the epidemic situation. The first phase, known as the "pre-outbreak phase," spanned from February 15 to February 28, 2022. During this period, only a small number of sporadic and locally transmitted cases were recorded, and people's daily activities remained largely unaffected. The period from February 1 to February 14 was excluded from our analysis as it is overlapped with the Chinese New Year holiday. The second phase is the "targeted interventions phase", covering the period from March 1 to March 31, when spatially targeted NPIs were deployed to suppress transmission. The third phase is the "citywide lockdown phase", covering the period from April 1 to April 30, when the entire city was in lockdown. The fourth phase is the "targeted lifting of interventions phase", covering the period from May 1 to May 31, when restrictions started to gradually scale down in specific areas of the city. The last phase is the "reopening phase", covering the period from June 1 to June 30, when policies started to be lifted throughout the entire city.

Frequency and Distance of Daily Trips. A trip was counted when a user switched to one or more new cell towers, until the user became stationary again (no further switch for approximately 30 min). We only consider trips between different cells of the grid. We defined as $T_{ij}(t)$ the number of trips from cell j to cell i at time t. The average number of trips per person at time t was thus defined as $\langle T\rangle(t) = T(t) / U(t)$, where $T(t) = \sum_{i\neq j} T_{ij}(t)$ represents the total number of trips at time t, and $U(t)$ represents the number of active users at time t (which dynamically changes over time due to the flow of travelers to and from Shanghai). We estimated aggregated mobility flows (directed) using a grid comprising 7,355 cells that covered the entire city of Shanghai, including all of its 16 districts and 216 subdistricts (*SI Appendix*, Fig. S1*A*). To quantify to what extent mobility changed during the outbreak, we compare the mobility during different epidemic phases to a baseline phase with pre-outbreak mobility. The geographical distance between the cell centroids is assumed to estimate the travel distance. Estimates were disaggregated by age, sex, day type (i.e., weekday and weekend), and time of the day (i.e., daytime and nighttime).

Definition of the Mobility Network and Community Detection. To investigate structural changes in the mobility network throughout various stages of the outbreak, we reconstructed the mobility network G_P for each phase P. In this network, each node represents a cell of the grid, with directed edges connecting nodes where users move between cell i and cell j. The degree of node i is then defined by $k_i = k_i^{in} + k_i^{out}$, where $k_i^{in} = \sum_j C_{ji}$, and $k_i^{out} = \sum_j C_{ij}$, where C_{ji} indicates whether node j is connected to node i or not (i.e., users travel from node j to node i). The average degree $\langle k\rangle$ is then calculated as $\langle k\rangle = \sum_{i=1}^{n} k_i / n$, where n is the number of nodes. The number of days in each phase P is denoted by D_P. Subsequently, the edge weights $w_{ij}(P)$ are calculated as the average daily number of trips between cells during this phase as $w_{ij}(P) = \sum_{t\in D_P} T_{ij}(t)/|D_P|$ We exclude edges whose average weight is below the threshold $w_{ij}(D) < 1$.

We used the Infomap method (23) to detect the community structures in the mobility network. Briefly, considering the sequence of communities visited by a random walker who will tend to linger within communities, the algorithm detects the community based on the probability distribution of random walks. A community partition is regarded as good if the description of that sequence requires relatively little information, in the sense of Shannon entropy, and the Infomap method is built to optimize the minimum description length of the random walk on the network. Compared with other methods, this approach retains the information about the directions and weights of the edges, which has the advantage of being flexible for finding community structures on large weighted and directed networks (31, 32). To assess community detection, we calculate the modularity (33). As an index of the difference of connectivity within a community versus between communities, a relatively lower modularity value indicates a higher strength of connections between different communities rather than within the same community.

The same methods were used to analyze the mobility networks and community structures by demographic characteristics by subsetting the dataset to consider only mobility flows for the analyzed population group.

Statistical Analysis. The mean number of daily trips per person and 95% CI (quantile interval) on the mean were calculated by bootstrap sampling for 100 times. Then number of daily trips per person among epidemic phases, age, sex, day type, and time of the day was compared by use of the two-sample t test. Similarly, a Kolmogorov–Smirnov test was used to compare the distribution of travel distance and degree of mobility network. The community detection process was performed 100 times to calculate the mean proportion of the area covered by the top 10 communities (α), the total number of identified communities (NC), the number of communities covering more than 10 cells ($NC_{g\geq 10}$), and their 95% CIs (quantile intervals). Then two-sample t test was used to compare the community structures of the mobility network. A Pearson correlation coefficient was estimated to test the association between epidemiologic metrics and mobility. The statistical significance level is set at 5%, which would be adjusted using Bonferroni correction for multiple comparisons.

Ethical Considerations. This study was approved by the institutional review board of the School of Public Health, Fudan University (IRB# 2022-05-0969).

Data, Materials, and Software Availability. The code is available at https://github.com/Juanjuan2023321/Shanghai-mobility-PNAS. Mobile phone data are proprietary and confidential. We obtained access to these data from the SmartSteps company controlled by China Unicom within the framework of the COVID-19 research project. To safeguard the privacy of the users, CSD was aggregated over time and space scale and by users' age group and sex (34). Raw individual-level and aggregated grid-level mobility data cannot be made publicly available to preserve privacy. However, readers can request the raw mobility data from the data provider—SmartSteps (34), and grid-level data to reproduce the findings of this study can be requested from the corresponding author.

ACKNOWLEDGMENTS. H.Y. acknowledges financial support from the Key Program of the National Natural Science Foundation of China (No. 82130093). X.L. is supported by the National Nature Science Foundation of China (No. 72025405, 72001211, 72301285, 82041020, 72088101), National Social Science Foundation of China (No. 22ZDA102), and the Hunan Science and Technology Plan Project (No. 2020TP1013). J. Zhang is supported by the Shanghai Rising-Star Program (No. 22QA1402300). S.T. is supported by the National Key R&D Program of China (No. 2022YFB3102600). M.C. is supported by the Natural Science Foundation of Hunan Province (No. 2023JJ40685).

Author affiliations: [a]Department of Epidemiology, School of Public Health, Key Laboratory of Public Health Safety, Ministry of Education, Fudan University, Shanghai 200032, China; [b]College of Systems Engineering, National University of Defense Technology, Changsha 410073, China; [c]Laboratory for Computational Epidemiology and Public Health, Department of Epidemiology and Biostatistics, Indiana University School of Public Health, Bloomington, IN 47405; and [d]Laboratory for the Modeling of Biological and Socio-technical Systems, Network Science Institute, Northeastern University, Boston, MA 02115

Author contributions: X.L. and H.Y. designed research; J. Zhang and S.T. performed research; J. Zhang, S.T., C.P., X.X., M.W., W. Lu, Y.W., B.S., M.C., A.G.K., Z.C., J. Zou, W. Li, W.Z., Y.L., and Y.Z. analyzed data; and J. Zhang, S.T., A.G.K., A.V., and M.A. wrote the paper.

1. J. Liu, M. Liu, W. Liang, The dynamic COVID-zero strategy in China. *China CDC Wkly.* **4**, 74–75 (2022).
2. Johns Hopkins University, COVID-19 dashboard (2023). https://coronavirus.jhu.edu/region/china. Accessed 29 July 2023.
3. Z. Chen *et al.*, Epidemiological characteristics and transmission dynamics of the outbreak caused by the SARS-CoV-2 Omicron variant in Shanghai, China: A descriptive study. *Lancet Reg. Health West. Pac.* **29**, 100592 (2022).
4. National Health Commission of the People's Republic of China, Update on the COVID-19 policys in China (2022). http://www.nhc.gov.cn/xcs/gzzcwj/202212/8278e7a7aee34e5bb378f0e0fc94e0f0.shtml. Accessed 20 July 2023.
5. C. Viboud *et al.*, Synchrony, waves, and spatial hierarchies in the spread of influenza. *Science* **312**, 447–451 (2006).
6. M. Chinazzi *et al.*, The effect of travel restrictions on the spread of the 2019 novel coronavirus (COVID-19) outbreak. *Science* **368**, 395–400 (2020).
7. A. Aleta *et al.*, Modelling the impact of testing, contact tracing and household quarantine on second waves of COVID-19. *Nat. Hum. Behav.* **4**, 964–971 (2020).
8. N. M. Ferguson *et al.*, Strategies for mitigating an influenza pandemic. *Nature* **442**, 448–452 (2006).
9. S. Merler, M. Ajelli, The role of population heterogeneity and human mobility in the spread of pandemic influenza. *Proc. Biol. Sci.* **277**, 557–565 (2010).
10. J. Sills *et al.*, Aggregated mobility data could help fight COVID-19. *Science* **368**, 145–146 (2020).
11. J. S. Jia *et al.*, Population flow drives spatio-temporal distribution of COVID-19 in China. *Nature* **582**, 389–394 (2020).
12. F. W. Crawford *et al.*, Impact of close interpersonal contact on COVID-19 incidence: Evidence from 1 year of mobile device data. *Sci. Adv.* **8**, eabi5499 (2022).
13. M. U. G. Kraemer *et al.*, The effect of human mobility and control measures on the COVID-19 epidemic in China. *Science* **368**, 493–497 (2020).
14. S. Chang *et al.*, Mobility network models of COVID-19 explain inequities and inform reopening. *Nature* **589**, 82–87 (2021).
15. P. Nouvellet *et al.*, Reduction in mobility and COVID-19 transmission. *Nat. Commun.* **12**, 1090 (2021).
16. W. Zheng *et al.*, Risk factors associated with the spatiotemporal spread of the SARS-CoV-2 Omicron BA. 2 variant–Shanghai Municipality, China, 2022.*China CDC Wkly*. **5**, 97–102 (2023).
17. F. Schlosser *et al.*, COVID-19 lockdown induces disease-mitigating structural changes in mobility networks. *Proc. Natl. Acad. Sci. U.S.A.* **117**, 32883–32890 (2020).
18. H. S. Badr *et al.*, Association between mobility patterns and COVID-19 transmission in the USA: A mathematical modelling study. *Lancet Infect. Dis.* **20**, 1247–1254 (2020).
19. S. Lai *et al.*, Effect of non-pharmaceutical interventions to contain COVID-19 in China. *Nature* **585**, 410–413 (2020).
20. E. Bertuzzo *et al.*, The geography of COVID-19 spread in Italy and implications for the relaxation of confinement measures. *Nat. Commun.* **11**, 4264 (2020).
21. C. Zhan, C. K. Tse, Y. Fu, Z. Lai, H. Zhang, Modeling and prediction of the 2019 coronavirus disease spreading in China incorporating human migration data. *PLoS One* **15**, e0241171 (2020).
22. V. Marziano *et al.*, Retrospective analysis of the Italian exit strategy from COVID-19 lockdown. *Proc. Natl. Acad. Sci. U.S.A.* **118**, e2019617118 (2021).
23. M. Rosvall, C. T. Bergstrom, Maps of random walks on complex networks reveal community structure. *Proc. Natl. Acad. Sci. U.S.A.* **105**, 1118–1123 (2008).
24. B. Klein *et al.*, Characterizing collective physical distancing in the US during the first nine months of the COVID-19 pandemic. arXiv [Preprint] (2022). https://doi.org/10.48550/arXiv.2212.08873. Accessed 25 September 2023.
25. A. Aleta *et al.*, Quantifying the importance and location of SARS-CoV-2 transmission events in large metropolitan areas. *Proc. Natl. Acad. Sci. U.S.A.* **119**, e2112182119 (2022).
26. China Internet Network Information Center, The 49th statistical report on China's internet development. https://www.cnnic.cn/NMediaFile/old_attach/P020220721404263787858.pdf. Accessed 30 July 2022.
27. G. Pullano, E. Valdano, N. Scarpa, S. Rubrichi, V. Colizza, Evaluating the effect of demographic factors, socioeconomic factors, and risk aversion on mobility during the COVID-19 epidemic in France under lockdown: A population-based study. *Lancet Digit. Health* **2**, e638–e649 (2020).
28. M. Manica *et al.*, Impact of tiered restrictions on human activities and the epidemiology of the second wave of COVID-19 in Italy. *Nat. Commun.* **12**, 4570 (2021).
29. H. Gibbs *et al.*, Detecting behavioural changes in human movement to inform the spatial scale of interventions against COVID-19. *PLoS Comput. Biol.* **17**, e1009162 (2021).
30. CEIC, China CN: Tel: Penetration rate: Mobile per 100 people: Shanghai. https://www.ceicdata.com.cn/en/china/telephone-number-of-mobile-per-100-people-by-region/cn-tel-penetration-rate-mobile-per-100-people-shanghai. Accessed 29 July 2023.
31. A. Lancichinetti, S. Fortunato, Community detection algorithms: A comparative analysis. *Phys. Rev. E* **80**, 056117 (2009).
32. S. Fortunato, Community detection in graphs. *Phys. Rep.* **486**, 75–174 (2010).
33. M. E. Newman, Fast algorithm for detecting community structure in networks. *Phys. Rev. E* **69**, 066133 (2004).
34. Smartsteps Data Technology Co., Ltd., Introduction of the mobile phone data provider: Smartsteps. http://www.smartsteps.com. Accessed 25 September 2023.